Numerical and Physical Modeling of Slope Stabilization with Large Diameter Shafts

A.G. Özcebe
European School for Advanced Studies in Reduction of Seismic Risk, ROSE School-IUSS, 27100 Pavia, Italy

C.G. Lai
Department of Civil Engineering and Architecture, University of Pavia, 27100 Pavia, Italy

V. Fioravante, D. Giretti, C. Prearo
University of Ferrara, Engineering Department, Via Saragat 1, 44100 Ferrara, Italy

SUMMARY
The static and dynamic stability of a uniformly fine-graded sandy slope reinforced with large diameter shafts (LDS) have been investigated by a series of geotechnical centrifuge tests at the ISMGEO laboratory in Seriate (BG), Italy. The main objective of the work is to build dynamic and static numerical models of the experiment able to satisfactorily capture the observed response of the physical model in laboratory and throw light into the behaviour of a slope stabilized with LDS under static and seismic loading and understand the response of this complex geotechnical-structural system. This paper presents the preliminary results of the numerical simulations of the dynamic tests, conducted by using the finite difference-based solver FLAC^{2D} (Itasca, 2011). Based on the results of the numerical-experimental studies, a simplified methodology will be proposed for the design of LDS aimed to reinforce unstable slopes under various geological and geotechnical conditions as a future development.

Keywords: seismic slope stability, large diameter shafts, numerical validation

1. INTRODUCTION

In order to develop a simplified framework in stabilizing seismic induced instability of landslides with large diameter shafts (LDS), EUCENTRE (European Centre for Training and Research in Earthquake Engineering) has been assigned a research project by Italian Department of Civil Protection. The aforementioned project involves both physical and numerical modelling, where the former serves for understanding the phenomenon for single combination of earthquake and slope geometry, and the latter is necessary to develop a simplified framework for slope stabilization with LDS depending on numerous different combinations of slope geometry and earthquake.

In order to eventually pass at the prototype scale, numerical modelling of the physical model (i.e. model of the model), is necessary to calibrate the parameters of the numerical model. A series of testing on physical model have been conducted using the ISMGEO (*Istituto Sperimentale Modelli Geotecnici*, Seriate – BG – Italy) geotechnical seismic centrifuge (IGC). Briefly, total of 6 tests have been performed for no shaft, single shaft and three shaft conditions under static and dynamic conditions, respectively.

For further and more complete information regarding the seismic centrifuge equipment and testing procedure, interested readers are referred to the companion paper (Static and dynamic centrifuge modelling of landslide stabilization with large-diameter shafts by Fioravante et al. 2012) in the conference proceedings. This paper is solely devoted to the details of numerical modelling of the physical model with its approximations and parameters. Accuracy and precision of the numerical model predictions are presented in terms of comparison of simulated and recorded accelerograms at 5 different points under plane strain dynamic conditions (namely for no-shaft, T.0D and three-shaft cases, T.3D).

2. BRIEF INFORMATION ON PHYSICAL AND NUMERICAL MODELS

2.1. Material models

2.1.1. Sand

FF sand (FFS), very fine and uniform silica powder, has been used in order to represent the unstable layer for the model scale tests performed at IGC. Grain size characteristics of FFS are summarized as in Table 2.1.

Table 2.1. Main geotechnical characteristics of FF sand

Parameter	*Symbol*	*Value*
Maximum dry unit weight	$\gamma_{d,max}$	14.78 kN/m^3
Minimum dry unit weight	$\gamma_{d,min}$	11.58 kN/m^3
Maximum void ratio	e_{max}	1.211
Minimum void ratio	e_{min}	0.732
Specific density	G_s	2.61
Mean particle size	D_{50}	0.093 mm
Uniformity coefficient	U_C	1.88
Friction angle at critical state	ϕ'_{cv}	33^o
Gravimetric water content at test	w_c	5 %
Relative density at preparation	D_R	30 %
5% water saturated unit weight	γ_s	13.00 kN/m^3

A well-calibrated equation for small strain shear stiffness of FFS as a function of void ratio and horizontal and vertical effective confining stresses is presented in Eq. (1.1) [Fioravante, 2000].

$$G_0 = C_G e^{2d} \left(\frac{\sigma'_v}{p_a} \right)^{2nv} \left(\frac{\sigma'_h}{p_a} \right)^{2nh} \tag{1.1}$$

where; d= non-dimensional exponent (=-0.4); nv= non-dimensional exponent (=0.136); nh= non-dimensional exponent (=0.084); C_G= dimensional matrix constant (=60 MPa); G_0= small strain (initial, maximum) shear stiffness; e= void ratio; p_a= atmospheric pressure (=101.3 kPa); σ'_h= horizontal effective stress; σ'_v= vertical effective stress.

Non-linear stress-strain relation in terms of shear modulus degradation curve is deducted from Young's modulus degradation curve measured from a series of triaxial tests on FF sand (Giretti, 2009). Figure 1 illustrates the shear modulus degradation curve (both discrete values and idealized curve).

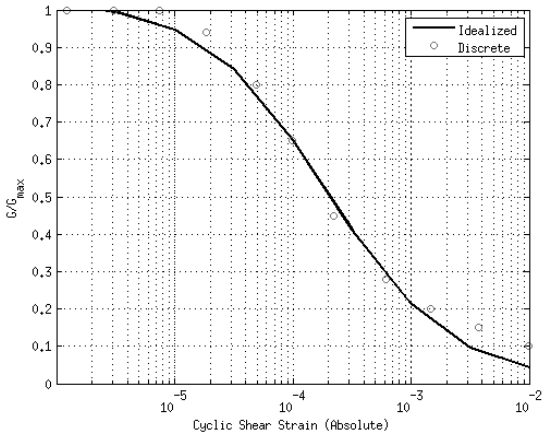

Figure 1. Shear modulus degradation curve used in numerical model (p'_0~50 kPa)

2.1.2. Stable bedrock

Stable bedrock is modelled in physical model by lightweight concrete having shear wave velocity ranging from ~900-1000 m/s, which is measured from the small strain elastic parameters (Young modulus and Poisson ratio).

2.1.3. Large diameter shaft (LDS)

The reinforcing large diameter shafts (LDS) are modelled by 200 mm long and 3.5 mm thick aluminium alloy (E_m= 70 GPa) hollow cylinders having external diameter 70 mm (EI_m= 2.837 10^{10} N.mm^2).

2.2. Physical model geometry and locations of accelerometers

Table 2.1. Geometrical dimensions of the physical models

	Parameter	*Value*
SLOPE GEOMETRY	Thickness, t	80 mm
	Elevation, z	325 mm
	Length, L	444 mm
	Slope angle, α	32^o
SHAFT GEOMETRY	External diameter, D_e	70 mm
	Internal diameter, D_i	63 mm
	Length of shaft, L_s	200 mm
	Average embedment, b	~80 mm
	Shaft spacing, s	105 mm

Table 2.1 and Figure 3 illustrate the geometry of the physical model. From Figure 3, locations of accelerometers may also be observed.

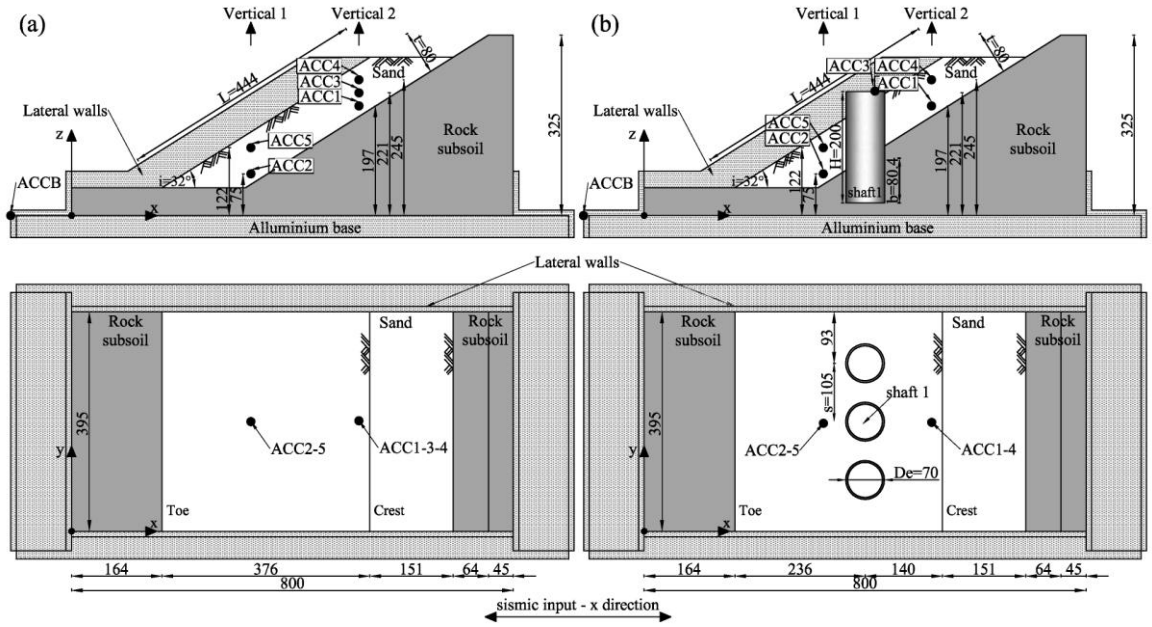

Figure 2. Geometry and accelerometer locations of physical model in dynamic centrifuge tests (T.0D and T.3D)

2.3. Properties of input acceleration and scaling

The input motion was selected from a set of 7, spectrum-compatible records specified for the Garfagnana territory, in Tuscany region, Italy, for outcropping rock conditions (see Fig 3) (Lai et al., 2008).

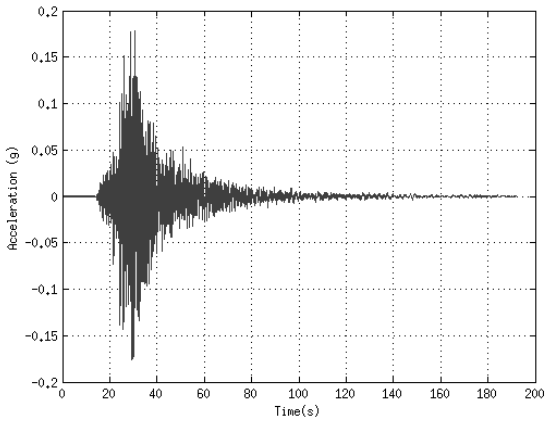

Figure 3. Acceleration-time history of the input motion

In a physical model geometrically scaled by a factor N and subjected to a centrifuge acceleration of Ng, both stresses and strains are scaled 1-to-1. Time in dynamic processes is scaled by a factor N whereas the acceleration is amplified by a factor N (Schofield 1980; Wood, 2004). The main similarity relationships between physical model and prototype scale are shown in Table 2.2.

Table 2.2. Similitude relations between physical model and prototype scale acceleration time histories

Quantity	*Prototype*	*Model*	*Quantity*	*Prototype*	*Model*
Length, L	N	1	Stress, σ	1	1
Velocity (projectile), v	1	1	Strain, ε	1	1
Acceleration, a	1	N	Mass Density, ρ	1	1
Mass, m	N^3	1	Time (dynamic), t_d	N	1
Force, F	N^2	1	Frequency, f	1	N

2.3. Numerical model

Figure 4 illustrates numerical model created in FLAC^{2D} for free-field dynamic (T.0D) and three-shaft dynamic (T.3D) simulations.

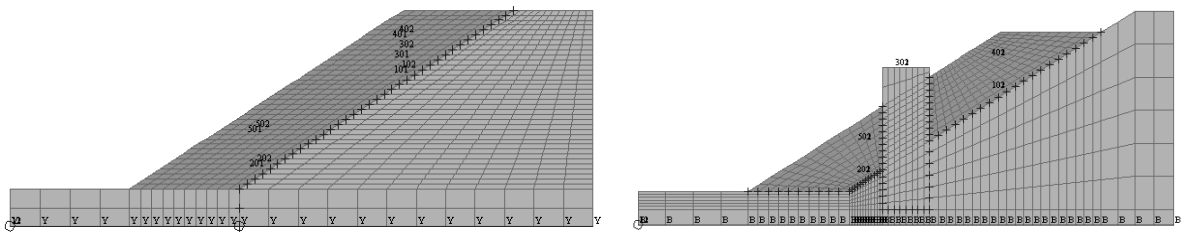

Figure 4. Numerical models for dynamic simulations
(left: free-field: T.0D, right: three-shaft: T.3D *for illustrative purposes only, not to the same scale*)

Cyclic non-linear constitutive model associated with elastic-perfectly plastic yielding type of inelasticity is the simplest and most widely used model which is being able to satisfactorily capture the response of slope instability. Owing to this reason, constitutive relation of unstable superficial sandy layer has been modelled with a cyclic non-linear model which fits the degradation curve shown in Figure 1 and having apparent cohesion (c_{app}) and internal friction (ϕ'=33^o) angle as yield parameters. Particular attention has been drawn to the partial saturation effects of 5% gravimetric water content on uniformly fine-graded FF-sand. It has been previously recognized and reported on different soil types that, partial saturation;

1. Increases the strength (Bishop, 1959; Fredlund et al., 1978)
2. Increases the small strain moduli (Cho and Santamarina, 2001; Sawangsuriya et al., 2008; and many others), and

3. May stiffen the soil matrix (Ng and Xu, 2012) so that makes the shear degradation curve more linear and reduces the amount of hysteretic damping at relatively smaller strains

In this work, all the effects of (1), (2), and (3) are considered in a simplified framework, which is going to be briefly discussed in the following sections.

2.3.1. Effect of partial saturation on soil strength

There is crystal clear evidence that partial saturation increases the soil strength due to osmotic and matric suction present in the pores. Bishop (1959) proposed an extension to Terzaghi's theory defined by a single stress state parameter and reformulated it as shown in Eq. (2.1).

$$\tau = c' + [(\sigma_n - u_a) + \chi(u_a - u_w)] \tan\phi' \tag{2.1}$$

where; τ= shear strength; c'= effective cohesion, ϕ'=angle of frictional resistance, $(\sigma_n - u_a)$= net normal stress, $(u_a - u_w)$= matric suction, χ= Bishop's effective stress.

Later, Fredlund et al. (1978) have proposed a more refined shear strength equation (Eq 2.2) for partially saturated soils which contains two independent stress state variables discussing that shear stress contribution due to matric suction need not to be constant for whole suction range (in fact, experimental evidence show that it is non-linear at relatively high levels of matric suction) as in the case of current study.

$$\tau = c' + (\sigma_n - u_a) \tan\phi' + (u_a - u_w) \tan\phi^b \tag{2.2}$$

For relatively small amount of matric suction tan $\phi^b \sim \chi \tan\phi'$, therefore Equations (2.1) and (2.2) converge. From these equations, apparent cohesion may be deducted as indicated in Equation (2.3).

$$c_{app} = \chi(u_a - u_w) \tan\phi' \tag{2.3}$$

Amount of c_{app} has been estimated by several means: (i) experimental back analysis of slope stability, (ii) conversion of grain size characteristics to SWCC (soil water characteristic curve), and (iii) numerical sensitivity analyses. Details of those are not going to be discussed in this manuscript. Special dedication will be made on another article. It can be briefly summarized that apparent cohesion has been found in the range of ~10-20 kPa.

2.3.2. Effect of partial saturation on initial soil stiffness

It has been clearly indicated by many authors that presence of partial saturation conditions increase the initial modulus of the soil matrix (Sawangsuriya et al., 2008; Cho and Santamarina, 2001; and many others). Knowing that the sand type under consideration has a well-calibrated stiffness equation (Eq. 1.1) to predict small strain shear modulus (G_0), the increment in shear stiffness has been modelled by an isotropic increase in effective stress due to partial saturation ($\Delta\sigma'_{ps}$) which is implemented into Eq. (1.1). Increase in effective stress due to partial saturation may be stated as in Eq (2.4) and found on the order of ~15-30 kPa.

$$\Delta\sigma'_{ps} = \frac{c_{app}}{\tan\phi'} \tag{2.4}$$

2.3.3. Effect of partial saturation on stress-strain curve

Compared to contributions to strength and initial stiffness, the effect of partial saturation to nonlinear monotonic or cyclic stress-strain curve is less investigated. Yet, there are recent experimental studies

showing that the presence of partial saturation stiffens the degradation at relatively low strains (Ng and Xu, 2012). Although this effect is not yet well represented, in this study it has been approximated with an increase in effective confining pressure (Eq. 2.4).

3. COMPARISON OF NUMERICAL PREDICTIONS WITH EXPERIMENTAL RESULTS

Two dimensional plane strain finite numerical models of T.0D and T.3D of the physical model have been created by using a FLAC^{2D} (Itasca, 2005; Itasca, 2011) according to the assumptions and material properties summarized in Section 2. Comparisons of numerical predictions with experimental results are provided in terms of recorded accelerations and their Fourier transforms at the accelerometers illustrated in Figure 2.

3.1. Numerical simulation for free-field test (T0.D)

3.1.1. Time domain comparisons

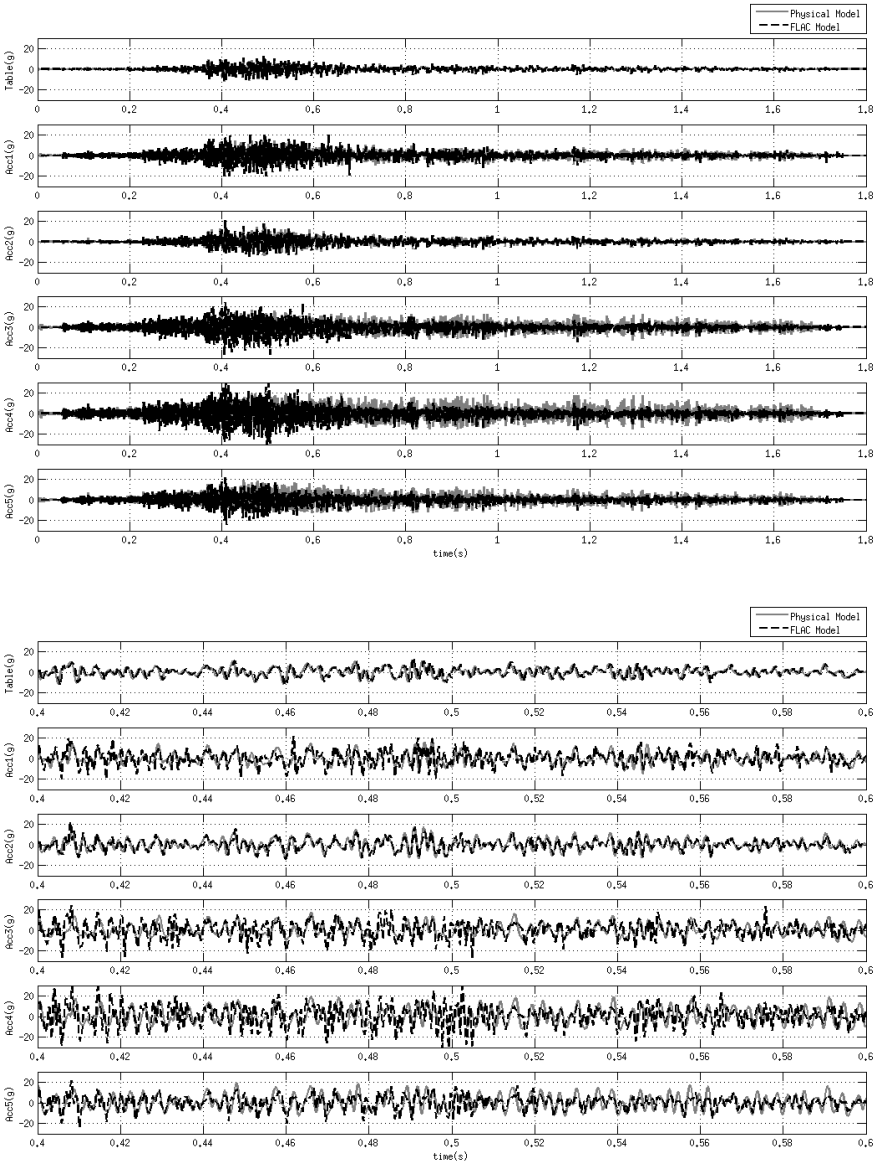

Figure 5. Comparison of acceleration time histories for T.0D in physical model scale (Table acc, Acc1, Acc2, Acc3, Acc4, and Acc5 respectively, filtered btw ~1-1000 Hz)

Figure 5 illustrates the comparison of simulated versus recorded acceleration-time histories. It is shown that the numerical simulations are capable to satisfactorily reproduce the general shape and amplitudes of the recorded waveforms. Since the acceleration amplitudes depend on the time dependent impedance ratio and trapped energy inside the soil layer, reproducing amplitudes correctly is a good indicator of the good performance of the constitutive model chosen to simulate the dynamic response of the sandy slope as well as of the correctness in the application of the complex boundary conditions of the centrifuge system and of the input motion.

Figure 5 also illustrates important features concerning the phases of recorded and simulated waveforms. In spite of little deviations in Acc4, it can be seen from Fig 5 that simulated and recorded acceleration-time histories are almost in-phase. Knowing that inelasticity, strain-dependent damping ratio and shear wave velocity of the sandy layer can significantly affect phase information of the records and may impose time delays (phase shifts) on the response, an almost in-phase reproduction of acceleration time histories implies that the model parameters were calibrated in acceptable ranges.

After the part with the significant energy of the input motion passes (t>0.7s), the rest of the acceleration-time history is causing smaller strain deformation on the soil and resulting in less amount of irreversible displacement compared to the part which carries the major energy. Due to the presence of excessive damping at small strains (*Fig 1*), the numerical model fails to reproduce amplitudes in Acc3, Acc4, and Acc5.

3.1.2. Frequency domain comparisons

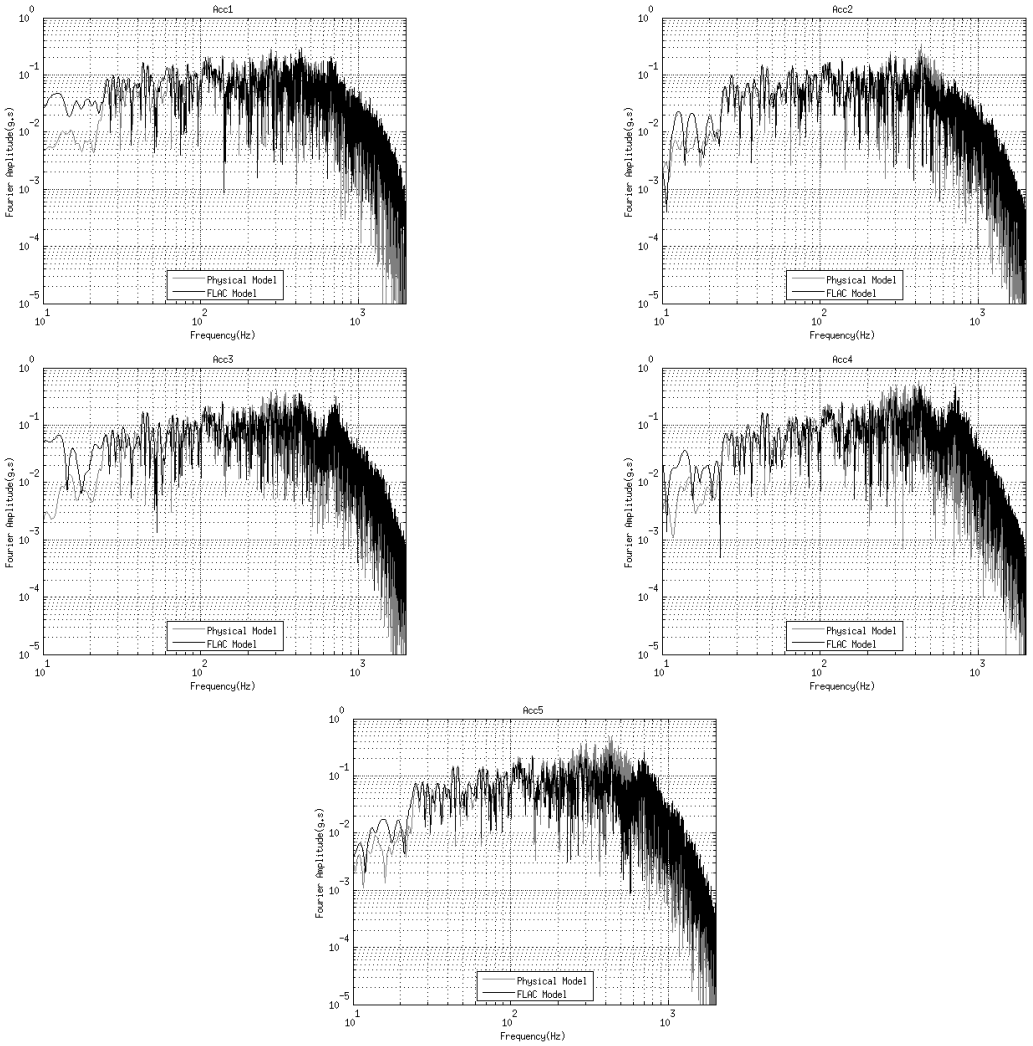

Figure 6. Comparison of acceleration time histories for T.0D in physical model scale, filtered btw ~1-1000 Hz

In order to show high amplitude and low amplitude motion equivalently, Fourier transforms have been performed on the time window from 0.2 to 0.9 s. Apart from the slight overestimation in Acc3 and Acc4 around f~750 Hz, frequency content of the simulated motions are very similar of those which were recorded at seismic centrifuge over a broad range of frequencies (f=10-2000 Hz in physical mode scale; f=0.2-40 Hz).

3.2. Numerical simulation for three-shaft test (T3.D)

3.2.1. Time domain comparisons

Figure 7 shows the results of four good and one poor numerical simulations. Experimental acceleration-time histories from 1 to 4 could satisfactorily be reproduced numerically. However, for Acc5 the numerical model fails to predict the response at that point.

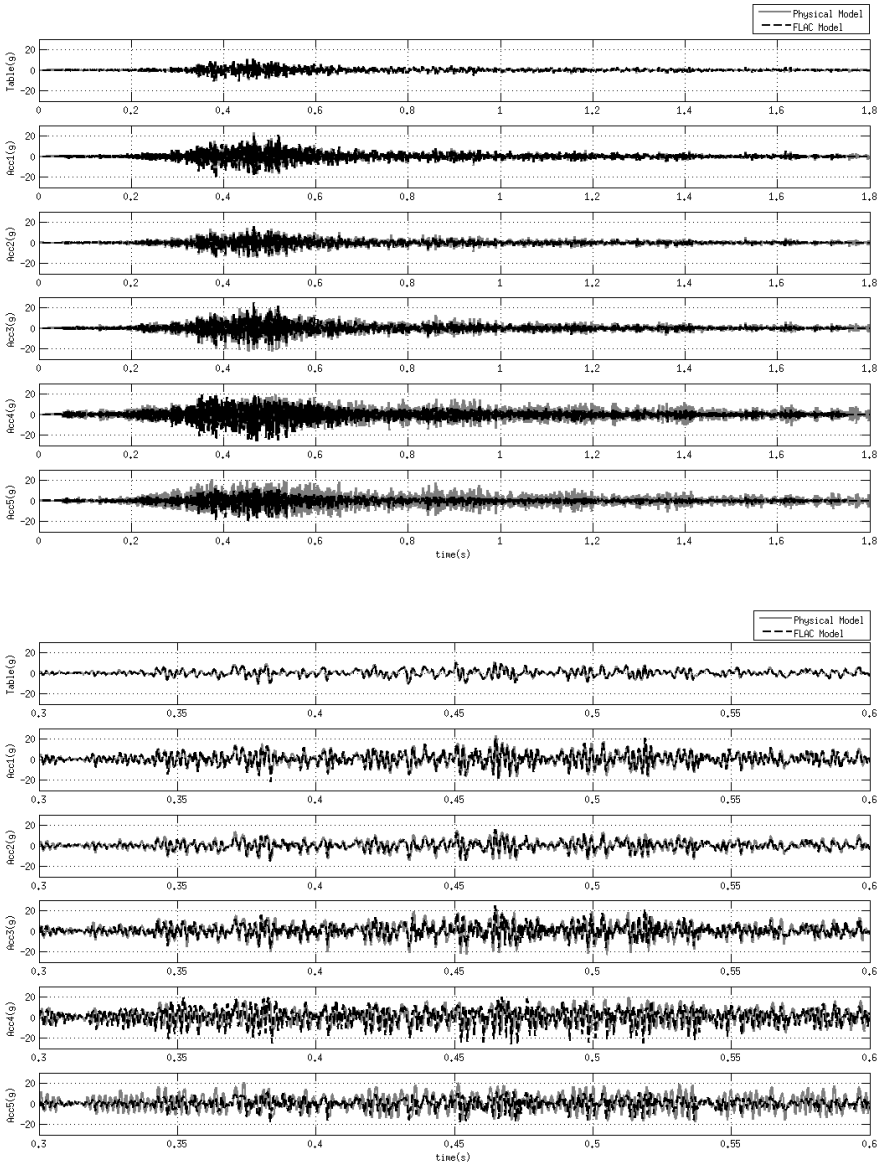

Figure 7. Comparison of acceleration time histories for T.3D in physical model scale
(Table acc, Acc1, Acc2, Acc3, Acc4, and Acc 5, respectively; filtered btw ~1-1000 Hz)

Different from the free-field test (T.0D), in the three-shaft test (T.3D) the location of the third accelerometer is not inside the soil layer, but on the shaft (*Fig 2*). Response history recorded at this

accelerometer depends on the natural period of the shaft, impedance ratio between the stable layer and the shaft and dynamic soil-shaft interaction. Therefore, a fairly good comparison in Acc 3 between synthetic and experimental records proves that all these aspects of the problem have been reproduced satisfactorily by the numerical model. Similarly to the free-field part, experimental records Acc1 to Acc4 are simulated in-phase with the experimental accelerograms. However the mismatch in Acc5 is significant and its deviation is predicted to be due to the higher damping of the simulated response compared to the observed experimental behaviour. The reason of this discrepancy has not yet been fully understood due to the complexity of the test and the possible causes are still being investigated.

3.2.2. Frequency domain comparisons

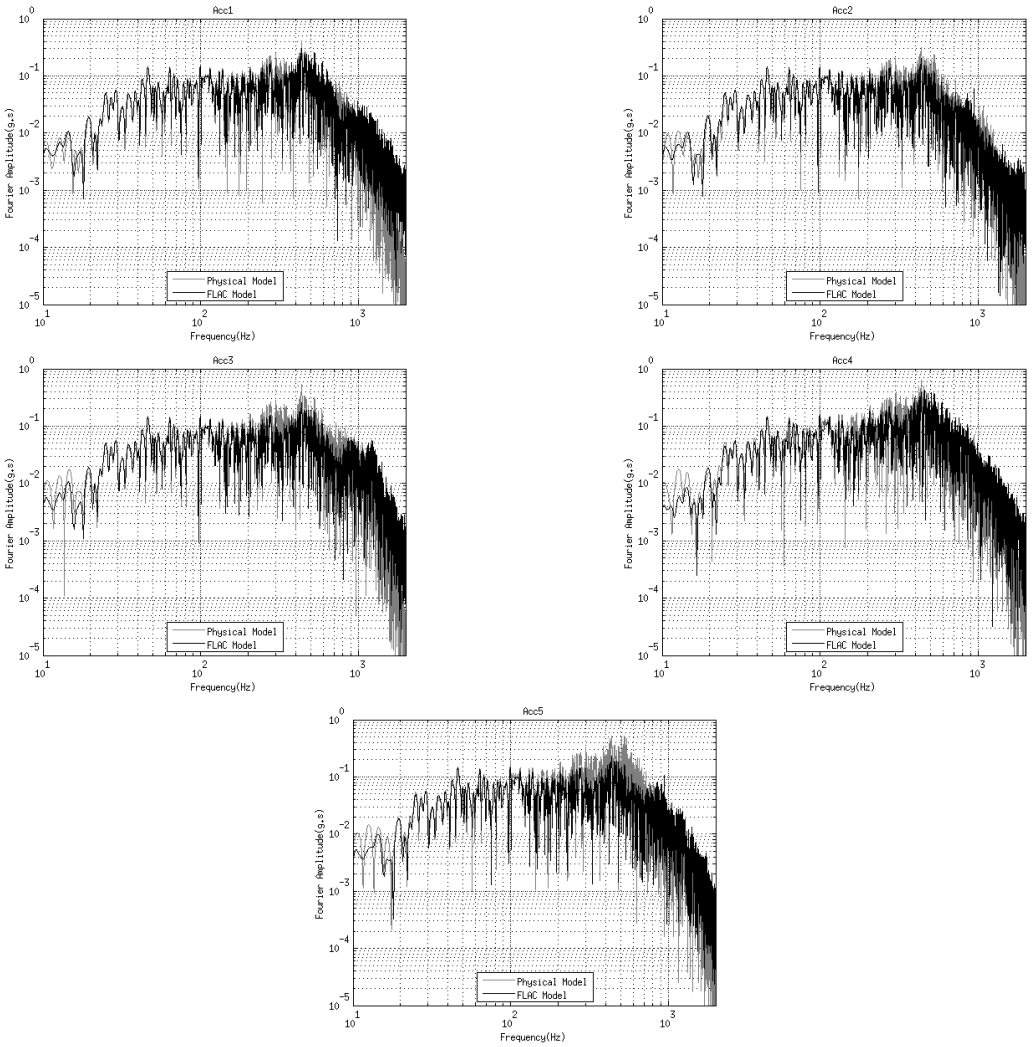

Figure 8. Comparison of acceleration time histories for T.3D in physical model scale, filtered btw ~1-1000 Hz

In order to show high amplitude and low amplitude motion equivalently, Fourier transforms have been performed on the time window of 0.2-0.95 s. Fig 8 shows that the frequency content of the simulated motion satisfactorily reproduce the lab recordings for Acc1 through 4. Similar to time-domain response, Acc5 significantly underestimates the frequency content, especially in the range of 300-800 Hz.

4. CONCLUSIONS AND DISCUSSIONS

In this manuscript, a simplified framework in simulating the effects of partial saturation using a hysteretic, non-linear constitutive model associated with Mohr-Coulomb failure criterion, has been

adopted and its verification with seismic centrifuge testing has been illustrated in a landslide stabilisation problem with large diameter shafts subjected to earthquake loading.

Experimental verifications have been carried in the time and frequency domains by comparing simulated versus recorded accelerograms at specific locations in the physical model. The results of this comparison are satisfactory. Although seismic performance of slopes is often measured by residual (irreversible) displacements exhibited by the soil mass at the end of seismic excitation, prediction of permanent displacements from double integration of the recorded accelerograms has not been carried out because the orientations of the accelerometers changed during the test. The sliding of the slope also caused a vertical component of motion that eventually caused a base rotation of the transducers. Although the baseline rotations of the accelerometers may have also introduced inaccuracies on the horizontal component of motion, these effects turned out to be negligible on the acceleration responses. However when it comes to integrate the accelerograms to yield the displacement responses, these inaccuracies got amplified yielding unreliable results.

ACKNOWLEDGEMENTS

The authors would like to express their gratitude to the Italian Department of Civil Protection of Italian Government and EUCENTRE, for having funded the research project (Progetto Esecutivo 2009-2012 – N. e6) and the ISMGEO staff for the assistance during the experimental working campaign, specifically Mr. Sergio Airoldi for his endless enthusiasm and very kind personality. First author is supported by a Ph.D. scholarship provided by IUSS/ROSE School. This financial support is also gratefully acknowledged.

REFERENCES

Itasca (2005). Fast Langragian Analysis of Continua v5. User's Guide, Itasca Consulting Group Inc, Minneapolis, USA.

Itasca (2011). Fast Langragian Analysis of Continua v7. User's Guide, Itasca Consulting Group Inc, Minneapolis, USA.

Giretti, D (2009). Modelling of piled raft foundations in sand. Dottorato di ricerca in scienze dell'ingegneria, Ciclo XXII. University of Ferrara, Italy.

Fioravante, V (2000). Anisotropy of small strain stiffness of Ticino and Kenya sands from seismic wave propagation measured in triaxial testing. *Soils and Foundations* **40:4**, 129-142.

Lai, C.G., Strobbia, C., Dall'Ara, A. (2008). Definizione dell'input sismico nei territory toscani della Lunigiana e Garfagnana. *Rivista Italiana di Geotecnica* **1**, 9-29.

Schofield, A.N. (1980). Cambridge Geotechnical Centrifuge Operations. *Geotechnique* **24:4**, 227-268.

Wood, D.M. (2004). Geotechnical modeling. Spon Press, Oxfordshire, UK.

Bishop, A.W. (1959). The principle of effective stress. *Tecnisk Ukeblad* **39**, 859–863.

Fredlund D.G., Morgenstern N.R., Widger R.A. (1978). The shear strength of unsaturated soils. *Canadian Geotechnical Journal* **15**, 313–321.

Cho, G.C., Santamarina, J.C. (2001). Unsaturated Particulate Materials – Particle Level Studies. *ASCE Geotechnical Journal* **127:1**, 84-96.

Sawangsuriya, A., Tuncer B.E., Bosscher, P.J. (2008). Modulus–suction–moisture relationship for compacted soils. *Canadian Geotechnical Journal* **45**, 973-983.

Ng, C.W.W., Xu, J. (2012). Effects of current suction ratio and recent suction history on small-strain behaviour of an unsaturated soil. *Canadian Geotechnical Journal* **49**, 226-243.